Eur. Phys. J. D **45**, 155–170 (2007)
DOI: 10.1140/epjd/e2007-00229-y

THE EUROPEAN PHYSICAL JOURNAL D

QED and relativistic corrections in superheavy elements

P. Indelicato[1,a], J.P. Santos[2], S. Boucard[1], and J.-P. Desclaux[3,b]

[1] Laboratoire Kastler Brossel, École Normale Supérieure; CNRS; Université P. et M. Curie - Paris 6, Case 74; 4, place Jussieu, 75252 Paris Cedex 05, France
[2] Centro de Física Atómica and Departamento de Física, Faculdade de Ciências e Tecnologia, Universidade Nova de Lisboa, Monte de Caparica, 2829-516 Caparica, Portugal
[3] 15 chemin du Billery, 38360 Sassenage, France

Received 15 January 2007 / Received in final form 31 May 2007
Published online 4 July 2007

Abstract. In this paper we review the different relativistic and QED contributions to energies, ionic radii, transition probabilities and Landé g-factors in super-heavy elements, with the help of the MultiConfiguration Dirac-Fock method (MCDF). The effects of taking into account the Breit interaction to all orders by including it in the self-consistent field process are demonstrated. State of the art radiative corrections are included in the calculation and discussed. We also study the non-relativistic limit of MCDF calculation and find that the non-relativistic offset can be unexpectedly large.

PACS. 31.30.Jv Relativistic and quantum electrodynamic effects in atoms and molecules – 31.25.Eb Electron correlation calculations for atoms and ions: ground state – 31.25.Jf Electron correlation calculations for atoms and ions: excited states – 32.70.Cs Oscillator strengths, lifetimes, transition moments

1 Introduction

In the last decades, accelerator-based experiments at GSI and Dubna have lead to the discovery of super-heavy elements up to $Z = 116$ and 118 [1] (for a recent review see [2]). Considerable theoretical work has been done to predict the ground configuration and the chemical properties of those superheavy elements. Relativistic Hartree-Fock has been used to predict the ground configuration properties of superheavy elements up to $Z = 184$ in the early 70's [3,4]. The Multiconfiguration Dirac-Fock (MCDF) method was used to predict orbital properties of elements up to $Z = 120$ [5], electron binding energies up to $Z = 118$ [6,7], and K-shell and L-shell ionization potentials for the superheavy elements with $Z = 112$, 114, 116, and 118 [8]. Ionization potential and radii of neutral and ionized bohrium ($Z = 107$) and hassium ($Z = 108$) have been evaluated with large scale MCDF calculations [9]. Kaldor and co-workers have employed the relativistic coupled-cluster method to predict ground state configuration, ionization potential, electron affinity, binding energy of the negative ion of several elements with $Z \geq 100$ [10–17].

Very recently, laser spectroscopy of several fermium ($Z = 100$) transitions has been performed, the spectroscopy of nobelium ($Z = 102$) is on the way [18–20], and large scale MCDF calculations of transition energies and rates have been performed by several authors for superheavy elements with $Z = 100$ [18,21], $Z = 102$ [21] and $Z = 103$ [22], which are in reasonable agreement with the fermium measurements.

There are however many unanswered questions, that need to be addressed in order to assess the accuracy and the limit of current theoretical methods. For inner-shells, or highly ionized systems, QED effects are very strong in superheavy elements, where the atomic number Z approaches the limit $Z\alpha \to 1$ ($\alpha = 1/137.036$ is the fine structure constant), at which the point-nucleus Dirac equation eigen-energies become singular for all $s_{1/2}$ and $p_{1/2}$ states (the energy depends on $\sqrt{\left(j+\frac{1}{2}\right)^2 - (Z\alpha)^2}$, where j is the total angular momentum). This means that all QED calculations must be performed for finite nuclei, and to all orders in $Z\alpha$. QED calculations for outer-shell are very difficult. At present, only the simplest one-electron, one-loop diagrams can be calculated, using model potentials to account for the presence of the other electrons. The evaluation of many-body effects, that remains large for neutral and quasi-neutral systems, is also made very difficult by the complex structure of these atoms, in which there may be several open shells. In that sense, methods based on Relativistic Many-Body Perturbation theory (RMBPT) and MCDF methods are complementary. The former one usually allowing for more

[a] e-mail: paul.indelicato@spectro.jussieu.fr
[b] e-mail: jean-paul.desclaux@wanadoo.fr

accurate results, but limited to (relativistic) closed shell systems minus one or plus one or at most two electrons, while the latter is completely general but convergence becomes problematic for large size configuration set, particularly if one wants to optimize all orbitals.

The paper is organized as follows. In Section 2 we present briefly the MCDF method, with emphasis on the specific features of the code we have been using, and we described the QED corrections that have been used in the calculations. In Section 3 we describe specific problems associated with the MCDF method (or more generally to all-order methods). We thus study the non-relativistic limit of the MCDF codes, and specific problems associated with high-Z. In Section 4 we study a number of systems from highly-charges ions to neutral atoms, for very large atomic numbers. The evaluation of atomic charge distribution size and Landé factors is performed in Section 5 and in Section 6 we state our conclusion.

2 Calculation of atomic wavefunctions and transition probabilities

2.1 The MCDF method

In this work, bound-states wavefunctions are calculated using the 2006 version of the Dirac-Fock program of Desclaux and Indelicato, named *mdfgme* [23]. Details on the Hamiltonian and the processes used to build the wavefunctions can be found elsewhere [24–27].

The total wavefunction is calculated with the help of the variational principle. The total energy of the atomic system is the eigenvalue of the equation

$$\mathcal{H}^{\text{no pair}}\Psi_{\Pi,J,M}(\ldots,\boldsymbol{r}_i,\ldots) = E_{\Pi,J,M}\Psi_{\Pi,J,M}(\ldots,\boldsymbol{r}_i,\ldots), \tag{1}$$

where Π is the parity, J is the total angular momentum eigenvalue, and M is the eigenvalue of its projection on the z-axis J_z. Here,

$$\mathcal{H}^{\text{no pair}} = \sum_{i=1}^{N}\mathcal{H}_D(r_i) + \sum_{i<j}V_{ij}(|\boldsymbol{r}_i - \boldsymbol{r}_j|), \tag{2}$$

where $\mathcal{H}_D$ is the one electron Dirac operator and V_{ij} is an operator representing the electron-electron interaction of order one in α. The expression of V_{ij} in Coulomb gauge, and in atomic units, is

$$V_{ij} = \frac{1}{r_{ij}} \tag{3a}$$

$$- \frac{\boldsymbol{\alpha}_i\cdot\boldsymbol{\alpha}_j}{r_{ij}} \tag{3b}$$

$$- \frac{\boldsymbol{\alpha}_i\cdot\boldsymbol{\alpha}_j}{r_{ij}}\left[\cos\left(\frac{\omega_{ij}r_{ij}}{c}\right)-1\right]$$

$$+ c^2(\boldsymbol{\alpha}_i\cdot\boldsymbol{\nabla}_i)(\boldsymbol{\alpha}_j\cdot\boldsymbol{\nabla}_j)\frac{\cos\left(\frac{\omega_{ij}r_{ij}}{c}\right)-1}{\omega_{ij}^2 r_{ij}}, \tag{3c}$$

where $r_{ij} = |\boldsymbol{r}_i - \boldsymbol{r}_j|$ is the inter-electronic distance, ω_{ij} is the energy of the exchanged photon between the two electrons, $\boldsymbol{\alpha}_i$ are the Dirac matrices and c is the speed of light. We use the Coulomb gauge as it has been demonstrated that it provides energies free from spurious contributions at the ladder approximation level and must be used in many-body atomic structure calculations [28,29].

The term (3a) represents the Coulomb interaction, the term (3b) is the Gaunt (magnetic) interaction, and the last two terms (3c) stand for the retardation operator. In this expression the $\boldsymbol{\nabla}$ operators act only on r_{ij} and not on the following wavefunctions.

By a series expansion of the operators in expressions (3b) and (3c) in powers of $\omega_{ij}r_{ij}/c \ll 1$ one obtains the Breit interaction, which includes the leading retardation contribution of order $1/c^2$. The Breit interaction is, then, the sum of the Gaunt interaction (3b) and the Breit retardation

$$B_{ij}^{\text{R}} = \frac{\boldsymbol{\alpha}_i\cdot\boldsymbol{\alpha}_j}{2r_{ij}} - \frac{(\boldsymbol{\alpha}_i\cdot\boldsymbol{r}_{ij})\,(\boldsymbol{\alpha}_j\cdot\boldsymbol{r}_{ij})}{2r_{ij}^3}. \tag{4}$$

In the many-body part of the calculation the electron-electron interaction is described by the sum of the Coulomb and the Breit interactions. Higher orders in $1/c$, deriving from the difference between expressions (3c) and (4) are treated here only as a first order perturbation. All calculations are done for finite nuclei using a Fermi distribution with a tickness parameter of 2.3 fm. The nuclear radii are taken or evaluated using formulas from reference [30].

The MCDF method is defined by the particular choice of a trial function to solve equation (1) as a linear combination of configuration state functions (CSF):

$$|\,\Psi_{\Pi,J,M}\rangle = \sum_{\nu=1}^{n} c_\nu\,|\nu,\Pi,J,M\rangle\,. \tag{5}$$

The CSF are also eigenfunctions of the parity Π, the total angular momentum J^2 and its projection J_z. The label ν stands for all other numbers (principal quantum number, ...) necessary to define unambiguously the CSF. The c_ν are called the mixing coefficients and are obtained by diagonalization of the Hamiltonian matrix coming from the minimization of the energy in equation (1) with respect to the c_ν. The CSF are antisymmetric products of one-electron wavefunctions expressed as linear combination of Slater determinants of Dirac 4-spinors

$$|\nu,\Pi,J,M\rangle = \sum_{i=1}^{N_\nu} d_i \begin{vmatrix} \psi_1^i(\boldsymbol{r}_1) & \cdots & \psi_m^i(\boldsymbol{r}_1) \\ \vdots & \ddots & \vdots \\ \psi_1^i(\boldsymbol{r}_m) & \cdots & \psi_m^i(\boldsymbol{r}_m) \end{vmatrix}, \tag{6}$$

where the ψ-s are the one-electron wavefunctions and the coefficients d_i are determined by requiring that the CSF is an eigenstate of J^2 and J_z. The one-electron wavefunctions are defined as

$$\psi(r) = \begin{pmatrix} \chi_\kappa^\mu(\Omega)P(r) \\ i\chi_{-\kappa}^\mu(\Omega)Q(r) \end{pmatrix}, \tag{7}$$

where χ_κ^μ is a two-component spinor, and P and Q are respectively the large and small component of the wavefunction.

Application of the variational principle leads to a set of integro-differential equations, which determines the radial wavefunctions and a Hamiltonian matrix, which provides the mixing coefficients c_ν by diagonalization. The *mdfgme* code provide the possibility to obtain wavefunctions and mixing coefficient with either only the Coulomb (3a) interaction used to obtain the differential equations and the Hamiltonian matrix that is diagonalized to obtain mixing coefficient or the full Breit operator (4). The convergence process is based on the self-consistent field process (SCF). For a given set of configurations, initial wavefunctions, obtained for example, with a Thomas-Fermi potential, are used to derive the Hamiltonian matrix and set of mixing coefficients. Direct and exchange potential are constructed for all orbitals, and the differential equations are solved. Then a new set of potentials is constructed and the whole process is repeated. Each time the largest variation of all wavefunction has been reduced by an order of magnitude, a new Hamiltonian matrix is build and diagonalized, and a new cycle is done.

The so-called Optimized Levels (OL) method was used to determine the wavefunction and energy for each state involved. This allow for a full relaxation of the initial and final states and provide much better energies and wavefunctions. However, in this method, spin-orbitals in the initial and final states are not orthogonal, since they have been optimized separately. The formalism to take in account the wavefunctions non-orthogonality in the transition probabilities calculation has been described by Löwdin [31] and Slater [32]. The matrix element of a one-electron operator O between two determinants belonging to the initial and final states can be written as

$$\langle \nu \Pi J M | \sum_{i=1}^{N} O(r_i) | \nu' \Pi' J' M' \rangle = \frac{1}{N!} \begin{vmatrix} \psi_1(r_1) & \cdots & \psi_m(r_1) \\ \vdots & \ddots & \vdots \\ \psi_1(r_m) & \cdots & \psi_m(r_m) \end{vmatrix} \times \sum_{i=1}^{m} O(r_i) \begin{vmatrix} \phi_1(r_1) & \cdots & \phi_m(r_1) \\ \vdots & \ddots & \vdots \\ \phi_1(r_m) & \cdots & \phi_m(r_m) \end{vmatrix}, \quad (8)$$

where the ψ_i belong to the initial state and the ϕ_i and primes belong to the final state. If $\psi = |n\kappa\mu\rangle$ and $\phi = |n'\kappa'\mu'\rangle$ are orthogonal, i.e., $\langle n\kappa\mu | n'\kappa'\mu' \rangle = \delta_{n,n'}\delta_{\kappa,\kappa'}\delta_{\mu,\mu'}$, the matrix element (8) reduces to one term $\langle \psi_i | O | \phi_i \rangle$ where i represents the only electron that does not have the same spin-orbital in the initial and final determinants. Since O is a one-electron operator, only one spin-orbital can change, otherwise the matrix element is zero. In contrast, when the orthogonality between initial and final states is not enforced, one gets [31,32]

$$\langle \nu \Pi J M | \sum_{i=1}^{N} O(r_i) | \nu' \Pi' J' M' \rangle = \sum_{i,j'} \langle \psi_i | O | \phi_{j'} \rangle \xi_{ij'} D_{ij'}, \quad (9)$$

where $D_{ij'}$ is the minor determinant obtained by crossing out the ith row and j'th column from the determinant of dimension $N \times N$, made of all possible overlaps $\langle \psi_k | \phi_{l'} \rangle$ and $\xi_{ij'} = \pm 1$ the associated phase factor.

The *mdfgme* code take into account non-orthogonality for all one-particle off-diagonal operators (hyperfine matrix elements, transition rates...). The overlap matrix is build and stored, and minor determinants are constructed, and calculated using standard LU decomposition.

2.2 Evaluation of QED corrections

In superheavy elements, the influence of radiative corrections must be carefully studied. Obviously the status of the inner orbital and of the outer ones is very different. It is not possible for the time being, to do a full QED treatment. Here we use the one-electron self-energy obtained using the method developed by Mohr [33,34]. These calculations have been extended first to the $n = 2$ shell [35,36] and then to the $n = 3$, $n = 4$ and $n = 5$ shells, for $|\kappa| \leq 2$ [37]. More recently, a new coordinate-space renormalization method has been developed by Indelicato and Mohr, that has allowed substantial gains in accuracy and ease of extension [38,39]. Of particular interest for the present work, is the extension of these calculation to arbitrary κ values and large principal quantum numbers [40]. All known values to date have been implemented in the 2006 version of the *mdfgme* code, including less accurate, inner shell ones, that covers the superheavy elements [41,42]. The self-energy of the $1s$, $2s$ and $2p_{1/2}$ states is corrected for finite nuclear size [43]. The self-energy screening is taken into account here by the Welton method [44,45], which reproduces very well other methods based on direct QED evaluation of the one-electron self-energy diagram with screened potentials [46–48]. Both methods however leave out reducible and vertex contributions. These two contributions, however, cancels out in the direct evaluation of the complete set of one-loop screened self-energy diagram with one photon exchange [49]. The advantages of screening method, on the other hand is that they go beyond one photon exchange, which may be important for the outer shells of neutral atoms. Recently special studies of outer-shell screening have been performed for alkali-like elements, using the multiple commutators method [50,51].

The comparison between the Welton model and the results from references [50,51] is presented in Table 1. This table confirms comparison with earlier work at lower Z. It shows that the use of a simple scaling law, as incorporated in GRASP 92 and earlier version of *mdfgme* does not provide correct values. This scaling law is obtained by comparing the mean value of the radial coordinate over Dirac-Fock radial wave-function $\langle r \rangle_{\mathrm{DF}}$ to the hydrogenic one $\langle r(Z_{\mathrm{eff}}) \rangle_{\mathrm{hydr.}}$. This allows to derive an effective atomic number Z_{eff} by solving $\langle r(Z_{\mathrm{eff}}) \rangle_{\mathrm{hydr.}} = \langle r \rangle_{\mathrm{DF}}$. One then use Z_{eff} to evaluate the self-energy screening from one-electron self-energy calculations. The superiority of the Welton model can be easily explained by noticing that the

Table 1. Self-energy and self-energy screening for element 111.

Level	$1s$	$7s$
SE (point nucl.)	848.23	3.627
Welton screening	−18.80	−3.283
Finite size	−50.37	−0.260
Total SE (DF)	779.06	0.084
Pyykkö et al. [51][a]		0.087
Pyykkö et al. [51][b]		0.095
$\langle r \rangle$ (GRASP) [52][c]		0.018

[a] Screening calculated using Dirac-Fock potential. [b] Screening calculated using Dirac-Slater potential fitted to $E_{DF.}$ [c] Use hydrogenic values with Z_{eff} obtained by solving $\langle r\,(Z_{\text{eff}})\rangle_{\text{hydr.}} = \langle r\,(Z_{\text{eff}})\rangle_{\text{DF.}}$

range of QED corrections is the electron Compton wavelength $\Lambda_C = \alpha$ a.u., while mean atomic orbital radii are dominated by contributions from the $\frac{n^2}{Z}$ a.u. range, which is much larger.

When dealing with very heavy elements in the limit $Z\alpha \to 1$, one should consider if perturbative QED is still a valid model. Unfortunately, we still lack the tools to answer this fundamental question. However, the use of *numerical all-order methods* may gives some partial answers. In particular they allow to include the leading contribution to vacuum polarization to all orders by adding the Uehling potential [53] to the MCDF differential equations. This possibility has been implemented in the *mdfgme* code as described in [54], with the help of reference [55]. It also allows to calculate the effect of vacuum polarization in quantities other than energies, like hyperfine structure shifts [54], Landé g-factors [56], or transition rates. It can also provides some hints on the oder of magnitude of QED effects on atomic wavefunction, orbital or atom radii, and electronic densities.

For high-Z, higher order QED corrections are also important. In the last decade, calculations have provided the complete set of values for two-loops, one-electron diagrams to all orders in $Z\alpha$ [57–61] and also low-Z expansions. All available data has been implemented in the mdfgme code. However, this data is limited to the $n \leq 2$ shells.

3 Limitation of the MCDF method

3.1 Non-relativistic limit

The success of relativistic calculations in high-Z elements atomic structure is impressive. It has been shown many times, that only a fully relativistic formalism and the use of a *fully* relativistic electron-electron interaction can reproduce the correct level ordering and energy in heavy systems. As a non-exhaustive list of example, we can cite the case of the $1s2p\ ^3\mathrm{P}_0$–$^3\mathrm{P}_1$ level crossing for $Z = 47$ in heliumlike systems [62–64], and the prediction of the $1s^22s2p\ ^3\mathrm{P}_0$–$^3\mathrm{P}_1$ inversion in Be-like iron [65], both due to relativistic effects and Breit interaction. Relativistic effects determine also the structure of the ground configuration of many systems, as was recognized for example in the study of lawrencium which has a $7p\ ^2\mathrm{P}$ in place of a $6d\ ^2\mathrm{D}$ configuration [66–68].

There is one caveat that must be taken into consideration when performing such calculations, that has been recognized in low-Z systems, but never explored in the superheavy elements region: it may sound rather paradoxical to investigate the nonrelativistic limit of MCDF and, more generally, of all-order calculations, when studying superheavy elements. Here we show, however, that there is a problem that has to be taken into account if one wants to obtain the correct fine structure splitting in all cases. We believe it is the first time this problem is recognized in the highly-relativistic limit.

This problem was first found many years ago, in systems like the fluorine isoelectronic sequence [69]: the nonrelativistic limit, obtained by doing $c \to \infty$ in a MCDF code, is not properly recovered. States with LSJ label $^{2S+1}L_J$ and identical L and S, and different J, which should have had the same energy in the non-relativistic limit do not. The energy difference between the levels of identical LS labels but different J is called the nonrelativistic (NR) offset. This offset leads to slightly incorrect fine structure in cases when a relativistic configuration has several non-relativistic parents (i.e., several states with one electron less, and different angular structure, that can recouple to give the same configuration). This effect can be large enough to affect comparison between theory and experiment. It should be noted that such a problem does not show if one works in the Extended Average Level (EAL) version of the MCDF. In this case a single wavefunction is used for all the members of a given multiplet, and the relaxation effects that are the source of the NR offset disappear, at the price of less accurate transition rates and energies, for a given configuration space.

Very recently, this non-relativistic problem was shown to be general to any all-order methods, in which subclasses of many-body diagrams are re-summed, without including all the diagrams relevant of a given order. In the MCDF method, in particular, one should add all configurations with single excitations of the kind $n\kappa \to n'\kappa$, that in principle, should have no effect on the energy in a nonrelativistic calculation, due to Brillouin's theorem [70]. In the iso-electronic sequence investigated up to now, this effects became less severe when going to higher Z, and it has thus never been considered in very heavy systems: in neutral, or quasi-neutral superheavy elements, the outer-shell structure can be complex, with several open shells, and thus many possible parents core configurations. It is then worthwhile to study if this problem could arise. We have studied a number of cases. As a first example we have studied neutral uranium. The ground state configuration is known to be $[\mathrm{Rn}]5f^36d7s^2\ ^5\mathrm{L}_6$. We have calculated all levels of the ground configuration with $J = 0$ to $J = 9$, both in normal conditions, and taking the speed of light to infinity in the code. The results are shown in Table 2 and Figure 1. There are two group of levels that can be

Table 2. Total relativistic energy [Ener. (BSC)], including all-order Breit and QED corrections, total non-relativistic energy [Ener. (NR)], and NR Offset for the ground configuration of uranium, relative to the $5f^3 6d 7s^2\ ^5\mathrm{L}_6$ energy, which is the lowest level of the configuration. Correlation has not been included. One can observe a splitting in the NR energy between the ^{5}H levels and the ^{5}L levels, which should be exactly degenerate. The fine-structure can be improved by subtract the NR offset from the relativistic energy.

Label	Ener. (BSC)	Ener. (NR)	NR offset
$^3\mathrm{P}_0$	1.25373	1.22751	
$^5\mathrm{D}_1$	1.62153	1.22803	
$^5\mathrm{G}_2$	1.28675	0.89836	
$^5\mathrm{H}_3$	0.91680	0.70185	0.0251
$^5\mathrm{H}_4$	1.05358	0.67678	0.0000
$^5\mathrm{K}_5$	0.14628	0.01169	
$^5\mathrm{L}_6$	0.00000	0.00000	0.0000
$^5\mathrm{L}_7$	0.42167	0.00181	0.0018
$^5\mathrm{L}_8$	0.85283	0.00333	0.0033
$^5\mathrm{L}_9$	1.28393	0.00284	0.0028

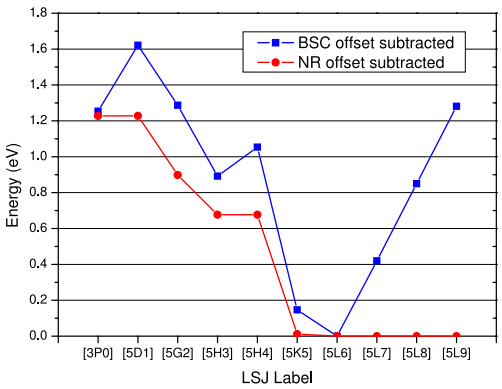

Fig. 1. (Color online) Non-relativistic offset on the ground configuration of uranium. "Ener. (BSC off. sub)": total MCDF energy, with all QED corrections, using the full Breit operator in the SCF process, relative to the $5f^3 6d 7s^2\ ^5\mathrm{L}_6$ energy to which the non-relativistic offset has been subtracted. "Ener. (NR off. sub)": Total non-relativistic energy, to which the non-relativistic offset for members of the same LS multiplet has been subtracted, relative to the $5f^3 6d 7s^2\ ^5\mathrm{L}_6$ energy. The two $^5\mathrm{H}_J$ and the four $^5\mathrm{L}_J$ levels have thus identical non-relativistic energy as it should be. Uncorrected energy and NR offset are displayed in Table 2.

affected by a NR offset: the $5f^3 6d 7s^2\ ^5\mathrm{H}_J$, $J = 3$, 4 and the $5f^3 6d 7s^2\ ^5\mathrm{L}_J$, $J = 6$ to $J = 9$. The non-relativistic offset is evaluated for both groups of levels as the difference between the energy of a configuration with a given J and the one for the configuration with the lower energy in the NR limit. Figure 1 and Table 2 clearly show a NR offset of 25 meV for the $^5\mathrm{H}_3$ and $^5\mathrm{H}_4$, and one of less than 1 meV for the four $^5\mathrm{L}_J$ levels. While it can be significant compared to the accuracy of a laser measurement, it is probably negligible compared to the accuracy of realistic correlation calculations.

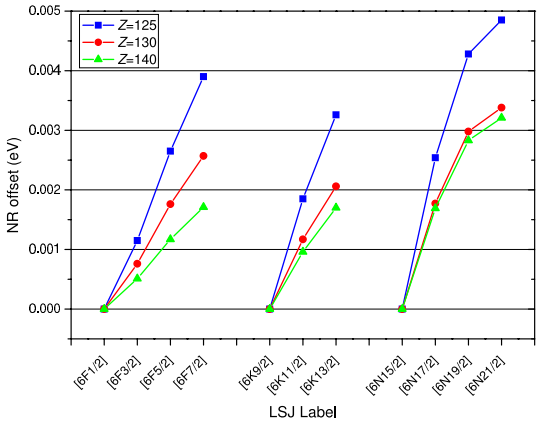

Fig. 2. (Color online) Non-relativistic offset for the $^6\mathrm{F}_J$, $^6\mathrm{K}_J$ and $^6\mathrm{N}_J$ LS configurations for the ground configuration of an atom with 125 electron. $Z = 125$, 130 and 1340 have been evaluated. This contribution should be negligible compared to correlation. For each LS group, the offset is evaluated by subtracting the lower energy of the group to the others.

In order to assess the generality of this problem, we have investigated several other characteristic systems. Element 125, for example, is the first element with a populated $5g$ orbital [3,4]. We have calculated the NR offset for a configuration with 125 electrons [Rn]-$5f^{14}6d^{10}7s^2 7p^6 8s^2 5g 6f^4$ and $Z = 125$, 135 and 140. The results are presented in Figure 2. We find three groups of levels with LSJ labels, four levels with label ^6F_J ($J = 1/2$ to $J = 7/2$), three levels with label ^6K_J ($J = 9/2$ to $J = 13/2$) and four levels with label ^6N_J ($J = 15/2$ to $J = 21/2$). The NR offset in each group is of the order of a few meV, while the (non-relativistic) energy difference between the two first groups is 0.19 eV, and between the first and the last groups is around 0.25 eV. The figure also shows that the NR offset gets smaller when Z increases as expected.

We have also investigated the lower excited states of a somewhat simpler system, element 118 (eka-radon). We have explored the [Rn]$5f^{14}6d^{10}7s^2 7p^5 8s$ which should exhibit no NR offset (it has single parent states) and [Rn]-$5f^{14}6d^{10}7s^2 7p^5 7d$. The results are presented in Table 3. As expected, the $7p^5 8s\ ^3\mathrm{P}_J$ states do not exhibit an NR offset, within our numerical accuracy. The $7p^5 7d\ ^3\mathrm{L}_J$ configurations however do have a strong NR offset, up to 0.8 eV, much larger than we expected from the other results presented above, and the largest ever observed. Clearly, such a large offset would render any calculation of the fine structure splitting of eka-radon useless, unless the results are corrected for the NR offset.

We would like to note that subtracting the NR offset is only a partial fix, since it was shown in reference [70] that not only the fine structure is affected, but also the level energy. The only possible solution are thus to do calculations with a large number of configurations, including all single excitations, or to use the EAL method. In view of the complexity of calculations on the superheavy elements, and of the extra convergence difficulties associated with the presence of Brillouin excitations, the first solution

Table 3. Non-relativistic offset on the lower excited configurations of eka-radon ($Z = 118$). For each member of a multiplet, as, e.g., $7p^5 7d\ ^3\mathrm{D}$, we evaluate the difference between the member with the lowest non-relativistic energy and the others. Non-relativistically, all member of a multiplet with identical LS labels should have an energy independent of the total angular momentum J.

J	$7p^5 7d\ ^3\mathrm{D}$	J	$7p^5 7d\ ^3\mathrm{F}$	J	$7p^5 7d\ ^3\mathrm{P}$	J	$7p^5 8s\ ^3\mathrm{P}$
1	0.801	2	0.335	0	0.000	0	0.000
2	0.000	3	0.000	1	0.002	1	0.002
3	0.336	4	0.000	2	0.802	2	0.002

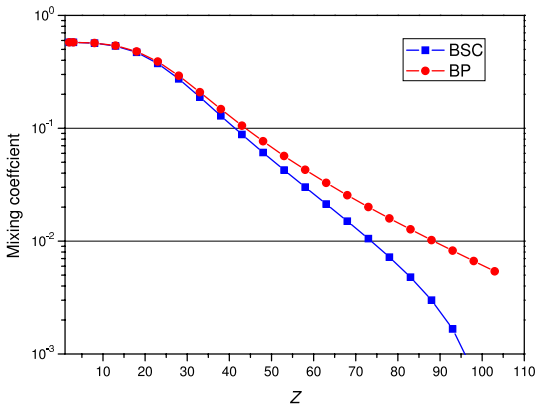

Fig. 3. (Color online) Variation with Z of mixing c_2 coefficient for the $1s2p\ ^3\mathrm{P}_1$ level of helium-like ions. BP: only the Coulomb interaction is used in the SCF process. BSC: the full Breit interaction is used in the SCF process.

is probably not very universal, but the second one should always work. In conclusion, we have shown for the first time, that it is important to check for the non-relativistic limit in super-heavy elements and to correct for the non-relativistic offset, as it can be large in some cases.

3.2 Effect of the all-order Breit operator on simple systems

The use of different form of the electron-electron interaction in the self-consistent field process has a profound qualitative influence on the behavior of variational calculations that goes beyond changes in energy. In particular the mixing coefficients between configurations contributing to intermediate coupling are strongly affected (and thus the values of many operators would be likewise affected). For example, let us examine the very simple case of the $1s2p\ ^3\mathrm{P}_1$ state in two-electron system. In a MCDF calculation, intermediate coupling is taken care of by calculating $\mid 1s2p\ ^3\mathrm{P}_1\rangle = c_1 \mid 1s2p_{1/2}\, J = 1\rangle + c_2 \mid 1s2p_{3/2}\, J = 1\rangle$. The evolution as a function of the atomic number Z of the c_2 coefficient, is plotted in Figure 3, with only the Coulomb interaction, or the full Breit interaction made self-consistent. The figure shows clearly that the inclusion of the Breit interaction in the SCF process lead to values of c_2 that are one order of magnitude lower at high-Z that when only the Coulomb interaction is included. It means that the JJ coupling limit is reached much faster. This has some influence even in the convergence of the calculation: as the exchange potential for the $2p_{3/2}$ orbital is proportional to $(c_1/c_2)^2$, it becomes very large, and the calculation does not converge. This can be traced back to a negative energy continuum problem. If we use the method described in reference [26] to solve for the $2p_{3/2}$, then convergence can be reached, provided the projection operator that suppress coupling between positive and negative energy solution of the Dirac equation is used. In Figure 4, the different contributions to the $1s2p\ ^3\mathrm{P}_1$ level energy are plotted at $Z = 40$. The minimum, which corresponds to the level energy, is obtained for a mixing coefficient (habitually obtained by diagonalization of the Hamiltonian matrix), $c_2 = 0.104$. The shape of the magnetic and retardation energy contribution, as observed on the figure, shows clearly that the curve used to find the minimum (which represents the sum of the contribution of the mean values of the operators in Eqs. (3a), (3b), and (4)) is shifted to the left compared to the pure Coulomb contribution. This explain why the mixing coefficients gets much smaller when using the Breit interaction in place of the Coulomb interaction in the SCF process. At high-Z this lead to an extra difficulty to achieve convergence: as can be seen in Figures 5 and 6, the minimum corresponding to the $1s2p\ ^3\mathrm{P}_1$ state (the one lower in energy) is very close to $c_2 = 0$. It thus sometimes happens during the convergence, that c_2 changes sign, leading to very tedious tuning of the convergence process. This is even worse for the $1s2p\ ^1\mathrm{P}_1$ state, because one is trying to reach the maximum energy. In that case the oscillation of the c_1 coefficient around zero are impossible to damp. Obviously, such problems will slowly disappear when going to neutral systems. For example, in neutral nobelium ($Z = 102$) c_2 changes only from 0.47250012 to 0.47316712.

4 Relativistic and QED effects on transition energies and probabilities

4.1 Beryllium isoectronic sequence correlation

It is interesting to investigate simple many-body system, that can be calculated accurately, to see which kind of highly relativistic effects can be expected in the limit $Z\alpha \to 1$. In that sense the beryllium isoelectronic sequence is an interesting model case, as it exhibit a very strong intrashell coupling between the $1s^2 2s^2 J = 0$ and $1s^2 2p_{1/2}^2 J = 0$ configurations, which are almost degenerate in energy. We thus calculated all contributions to the energy, with and without including the vacuum polarization and Breit interaction in the SCF process. From this we could deduce the loop-after-loop Uehling contribution to the total energy, and the intrashell correlation. Most quantities contributing to the total energy do not exhibit any specific behavior when $Z\alpha \to 1$. However, a major changes in behavior of the system occurs around $Z = 125$ as shown in Figure 7. One can see that the ground state, which is $1s^2 2s^2\ J = 0$ at lower Z, becomes $1s^2 2p_{1/2}^2\ J = 0$.

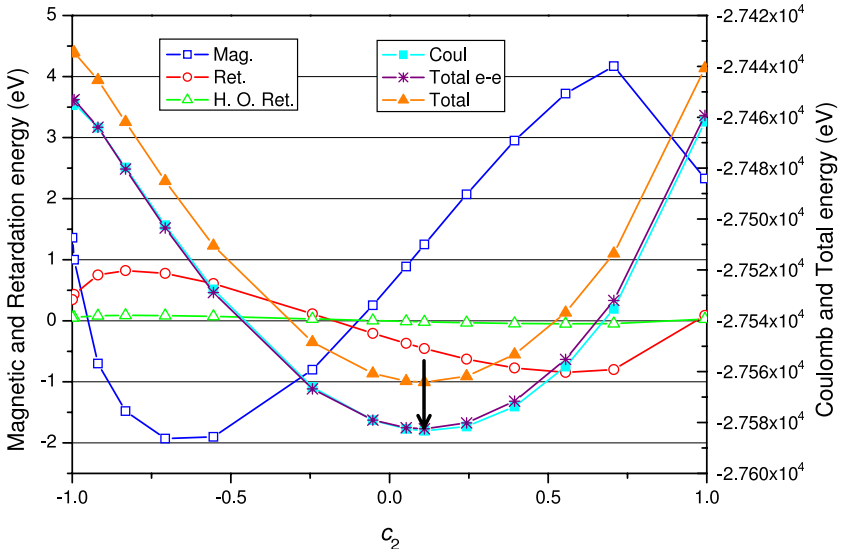

Fig. 4. (Color online) Variation of the different contributions to the energy as a function of the mixing coefficient c_2, for the $1s2p\ ^3\mathrm{P}_1$ level at $Z = 40$. The arrow indicates the position of the $1s2p\ ^3\mathrm{P}_1$ energy, at the minimum around $c_2 = 0.104$. Left axis: "Mag.": magnetic energy, equation (3b). "Ret.": Breit retardation, equation (4). "H.O. Ret.": higher-order retardation. Right axis: "Coul.": Coulomb energy equation (3a). "Total e-e": sum of the 4 preceding contributions. "Total": total level energy including all QED corrections.

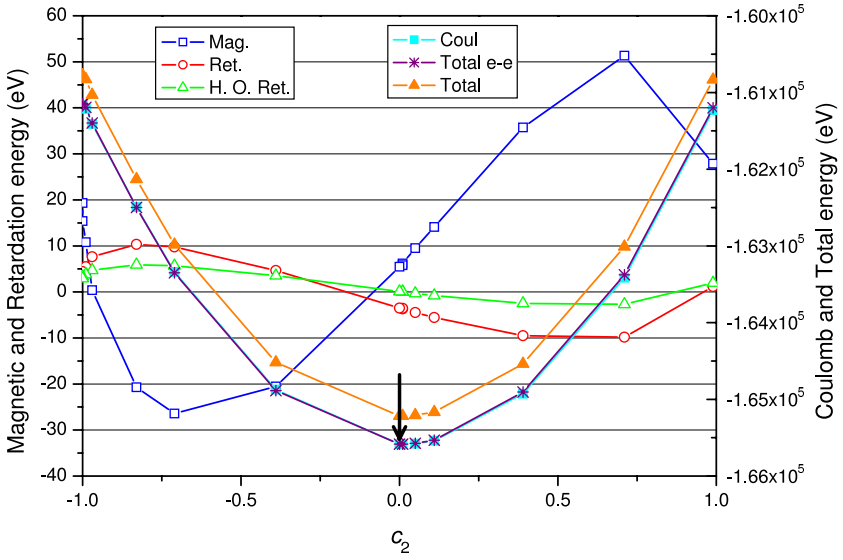

Fig. 5. (Color online) Variation of the different contributions to the energy as a function of the mixing coefficient c_2, for the $1s2p\ ^3\mathrm{P}_1$ level at $Z = 92$. The arrow indicates the position of the $1s2p\ ^3\mathrm{P}_1$ energy, at the minimum around $c_2 = 0.002$. Left axis: "Mag.": magnetic energy, equation (3b). "Ret.": Breit retardation, equation (4). "H.O. Ret.": higher-order retardation. Right axis: "Coul.": Coulomb energy equation (3a). "Total e-e": sum of the 4 preceding contributions. "Total": total level energy including all QED corrections.

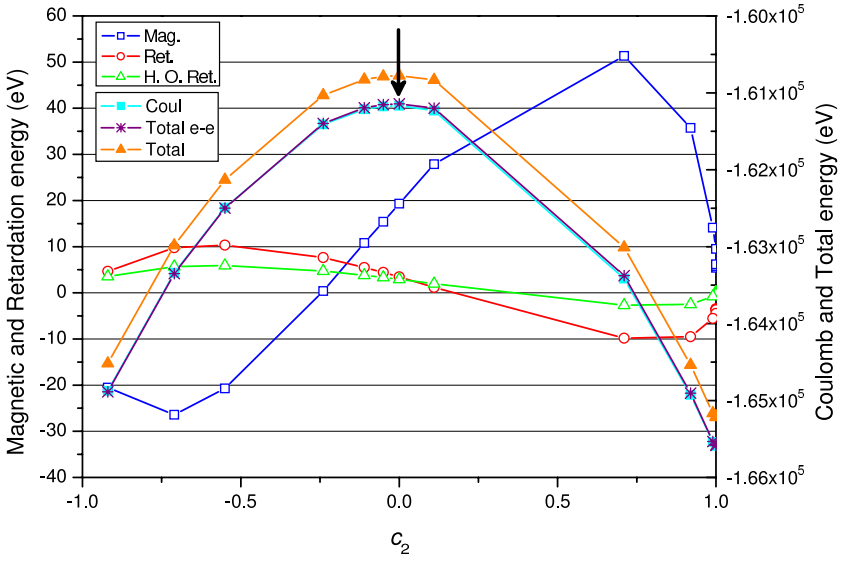

Fig. 6. (Color online) Variation of the different contributions to the energy as a function of the mixing coefficient c_1, for the $1s2p\ ^1\mathrm{P}_1$ level at $Z = 92$. The arrow indicates the position of the $1s2p\ ^1\mathrm{P}_1$ energy, at the *maximum* around $c_1 = 0.002$. Left axis: "Mag.": Magnetic energy, equation (3b). "Ret.": Breit retardation, equation (4). "H.O. Ret.": higher-order retardation. Right axis: "Coul.": Coulomb energy equation (3a). "Total e-e": sum of the 4 preceding contributions. "Total": total level energy including all QED corrections.

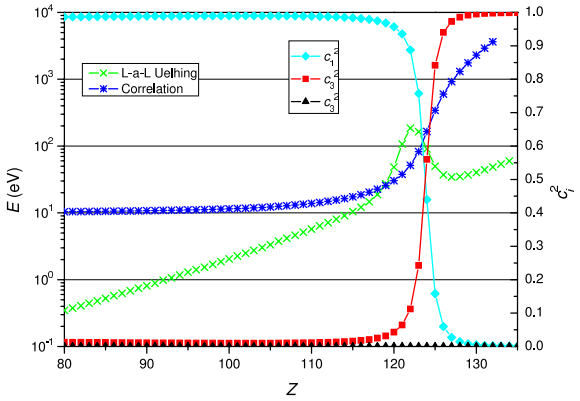

Fig. 7. (Color online) Loop-after-loop Uehling contribution to berylliumlike ions ground state energy (changed of sign), obtained by including the Uehling potential in the SCF. The intrashell correlation energy is also plotted (left axis), as well as the square of the mixing coefficients of the $1s^2 2s^2\ J = 0$, $1s^2 2p_{1/2}^2\ J = 0$ and $1s^2 2p_{3/2}^2\ J = 0$ configurations (right axis).

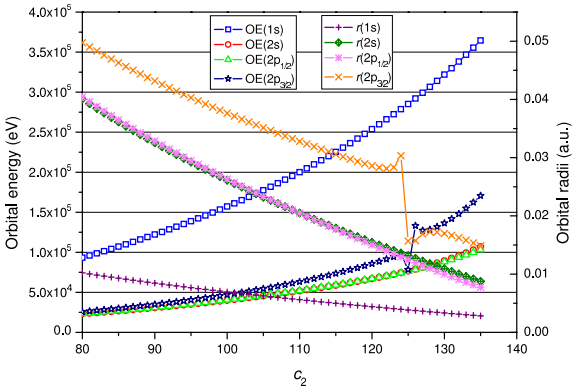

Fig. 8. (Color online) Orbital radii (right axis) and one-electron energies (left axis) for Be-like ions.

This can be seen on the mixing coefficients as plotted in Figure 7. This translates into a strong increase in the loop-after-loop vacuum polarization contribution. Obviously, if we were able to evaluate other second-order QED calculation than loop-after-loop vacuum polarization, including off-diagonal two-electron self-energy matrix elements for quasi-degenerate state, following recent work on heliumlike systems [71–73], there could be more unexpected effects to observe.

While not displaying such a feature, the total correlation energy increases strongly, reaching up to 3.6 keV. One can observe effects on other properties of the atom, like orbital energies and mean orbital radius. Figure 8 shows that, in the same atomic number range when the ground state changes of structure, the $2p_{3/2}$ orbital radius and energy exhibit a very strong change. The behavior of the ground state must be connected to the fact that the small component of $2p_{1/2}$ orbitals, as can be seen from equation (7), has a s behavior, and the ratio between small and large component is of order $Z\alpha$. It is thus understandable that such effects could occurs when $Z\alpha \to 1$. It should be noted that this effects happens even with a pure Coulomb electron-electron interaction, which is one more proof it is only connected with the behavior of the one-electron wavefunctions. We investigated the similar case of the magnesiumlike sequence, which exhibit strong intrashell coupling between the $3s$, $3p$ and $3d$ orbitals, but we could not observe any effect on energies in this range of Z. However the $[\mathrm{Ne}]3p_{1/2}^2$ mixing coefficient started to increase faster around $Z = 128$, but convergence problems prohibited us to investigate higher Z.

4.2 Relativistic correlations on the neon isoelectronic sequence

Calculating completely correlated energies can be performed only on relatively small systems. Neonlike ions, with 10 electrons are a small enough system that can be calculated with rather large basis sets. We have extended the calculation performed in reference [7] to superheavy elements ($Z = 134$). All 10 electrons are excited to all virtual orbitals up to a maximum $n\ell$, that is varied from $3d$ to $6h$. The results are presented in Table 4 and plotted in Figure 9. The trend found up to $Z = 94$ in reference [7] extend smoothly to larger Z, but is enhanced. The total correlation energy becomes very large. It doubles when going from $Z = 95$ to $Z = 134$, the highest Z for which convergence could be reached. The speed of convergence as a function of $n\ell$ does not change with increasing Z.

Table 4. Total correlation energy for neonlike ions, with the Breit interaction included in the SCF, as a function of the most excited orbital included in the basis set.

Z	all $\to 3d$	all $\to 4f$	all $\to 5g$	all $\to 6h$
10	−5.911	−8.306	−9.339	−9.709
15	−5.989	−8.712	−9.838	−10.280
25	−6.374	−9.310	−10.494	−10.967
35	−6.710	−9.850	−11.099	−11.609
45	−7.074	−10.482	−11.816	−12.372
55	−7.515	−11.269	−12.710	−13.322
65	−8.067	−12.260	−13.833	−14.511
75	−8.752	−13.375	−15.247	−16.007
85	−9.772	−15.119	−17.056	−17.916
95	−11.160	−17.231	−19.429	−20.415
105	−13.205	−20.146	−22.700	−23.853
114	−15.975	−23.966	−26.974	−28.332
124	−21.222	−30.897	−34.694	−36.389
130	−26.714	−37.777	−42.304	−44.300
134	−32.248	−44.412	−49.598	−51.860

4.3 Transition energies and probabilities in nobelium and element 118 (eka-radon)

In this section we study the different contributions to the energy and transition probabilities of nobelium ($Z = 102$) and eka-radon ($Z = 118$). Nobelium is the next candidate for measurement of its first excited levels transition energy by laser spectroscopy. Large scale calculations have been

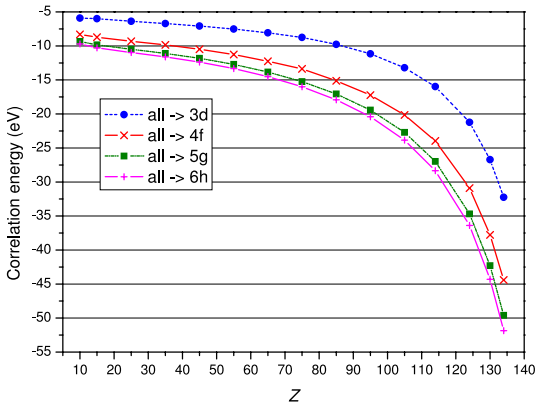

Fig. 9. (Color online) Total correlation energy for neonlike ions, with the Breit interaction included in the SCF, as a function of the most excited orbital included in the basis set.

performed recently [21]. Here we examine a number of corrections not considered in reference [21]. For the $7s^2\ {}^1\mathrm{S}_0$ ground state, we did a MCDF calculation taking into account all single and double excitations, except the ones corresponding to the Brillouin theorem, from the $5f$ and $7s$ shells to the $7p$, and $6d$ shells (48 jj configurations). For the excited states we included excitations from $5f$, $7s$ and $7p$ shells to the $7p$ and $6d$ ones. This leads to 671 jj configurations for the $7s7p\ {}^3\mathrm{P}_1$ and $7s7p\ {}^1\mathrm{P}_1$ states and 981 for $7s7p\ {}^3\mathrm{P}_2$. The results of this calculation are presented in Table 5 for the transition energies and in Table 6 for transition probabilities. It is clear from these two tables that many contributions that are important for level energies are completely negligible for transition probabilities in this case. This is not true for highly charged ions, even at much lower Z. In particular two-loop QED corrections, even though many of them have not been calculated from $n > 2$, should remain completely negligible, since they will be of the same order of magnitude as the loop-after-loop and Källèn and Sabry contributions. The self-energy screening is almost exactly compensating the self-energy, but leaves a contribution that should be visible if one can calculate correlation well enough. At the present level of accuracy, calculation of the pure Coulomb correlation is the real challenge as it requires considerable effort on the size of configuration space.

The transition probabilities in Table 6 have been evaluated with different approximation, using theoretical energies. Here the choice of the wavefunction optimization technique has a sizeable effect. It remains small compared to correlation, but still at the level of 0.2%. We also investigated the effect of using fully relaxed orbitals on both initial and final state. In particular we checked at the Dirac-Fock level of approximation, what is the order of magnitude of taking into account non-orthogonality between initial and final state orbitals. We found 2.2% for the ${}^3\mathrm{P}_1 \rightarrow {}^1\mathrm{S}_0$ transition, 0.014% for the ${}^1P_1 \rightarrow {}^1S_0$ transition and −0.025% for the ${}^3\mathrm{P}_2 \rightarrow {}^1\mathrm{S}_0$. For calculations between correlated wavefunctions, it is anyway important to evaluate the matrix elements for off-diagonal operators, taking account non-orthogonalities between initial and final state orbitals, as it can change dramatically the contribution of a given CSF, since overlaps between correlations orbitals in initial and final states can be very different from either one or zero.

Table 5. Transition energies for the lower energy levels of nobelium (eV). Coul.: DF Coulomb energy. Mag. (pert), Ret. (pert.), Higher order ret. (pert.): contribution of the Magnetic, Breit retardation and higher-order retardation in first order of perturbation. All order Breit: effect of including the full Breit interaction in the SCF. Coul. Corr.: Coulomb correlation. Breit Corr.: contribution of all Breit terms to the correlation energy. Self-energy (FS): self-energy and finite size correction. Self-energy screening: Welton approximation to self-energy screening. Vac. Pol. (Uehling): mean value of the Uehling potential (order $\alpha(Z\alpha)$). VP (muons, Uehling): vacuum polarization due to muon loops. VP Wichman and Kroll: correction to the Uehling potential (order $\alpha(Z\alpha)^3$). Loop-after-loop V11: iterated Uehling contribution to all orders. VP (Källèn et Sabry): two-loop contributions to vacuum polarization. Other 2nd order QED: sum of two-loop QED corrections not accounted for in the two previous one. Recoil: sum of lowest order recoil corrections (see, e.g., [74]). The number of digits presented in the table is not physically significant, but is necessary to show the size of some contributions. The physical accuracy is not better than 1 digits.

Contribution	${}^3\mathrm{P}_1 \rightarrow {}^1\mathrm{S}_0$	${}^1\mathrm{P}_1 \rightarrow {}^1\mathrm{S}_0$	${}^3\mathrm{P}_2 \rightarrow {}^1\mathrm{S}_0$
Coul.	1.69909	3.20051	2.19931
Mag. (pert)	0.00070	−0.00420	−0.00347
Ret. (pert.)	−0.00048	0.00005	−0.00058
Higher order ret. (pert.)	−0.00119	0.05048	−0.00231
All order Breit (pert)	0.00002	−0.05877	0.00003
Coul. Corr.	0.59560	0.60414	0.55545
Breit Corr.	−0.00208	−0.00229	−0.00194
Self-energy (FS)	−1.60884	−1.72025	−1.76085
Self-energy screening	1.59030	1.72940	1.74228
Vac. Pol. (Uehling)	0.00610	0.00435	0.00648
VP (muons. Uehling)	0.00000	0.00000	0.00000
VP Wichman and Kroll	−0.00030	−0.00019	−0.00033
Loop-after-loop Uehl.	0.00002	0.00012	0.00003
VP (Källèn and Sabry)	0.00004	0.00002	0.00005
Other 2nd order QED	0.00000	0.00000	0.00000
Recoil	−0.00082	−0.00081	−0.00082
Total	2.28	3.80	2.73
Ref. [21] II	2.34	3.49	
Ref. [21] I	2.60	3.36	

We have also calculated several transition energies and rates for element 118, which are displayed in Table 7. For the most intense $7p^5 7d \rightarrow 7s^2 7p^6$ transitions and for the $7p^5 8s \rightarrow 7s^2 7p^6$ transitions we did a MCDF calculation, taking into account all single and double excitations, (except the ones corresponding to the Brillouin theorem) from the $7s$ and $7p$ shells to the $7d$ and $6f$ shells for the $7p^6\ {}^1\mathrm{S}_0$ ground state (38 jj configurations) and for the $7p^5 7d$ excited states (657 jj configurations), and from the $7p$ and $8s$ shells to the $7d$ and $6f$ shells for the $7p^5 8s$ excited states (151 jj configurations).

The transition energy was calculated for some of these transitions, with and without including the vacuum polarization and Breit interaction in the SCF process, and we concluded that the transition energy is not significantly

Table 6. Effect of correlation, Breit interaction and all order vacuum polarization on transition probabilities of nobelium. DF: Dirac-Fock. VP: vacuum polarization. ex.: excitation.

initial final	$7s7p\ ^{2S+1}\mathrm{P}_J$ DF $\rightarrow 7s^2\ ^1\mathrm{S}_0$ DF	$7s7p\ ^{2S+1}\mathrm{P}_J$ ex. $7s$, $7p \rightarrow 7p$, $6d$ $\rightarrow 7s^2\ ^1\mathrm{S}_0$ ex. $7s \rightarrow 7p$, $6d$	$7s7p\ ^{2S+1}\mathrm{P}_J$ ex. $5f$, $7s$, $7p \rightarrow 7s$, $7p$, $6d$ $\rightarrow 7s^2\ ^1\mathrm{S}_0$ ex. $7s \rightarrow 7p$, $6d$
$7s7p\ ^3\mathrm{P}_1 \rightarrow 7s^2\ ^1\mathrm{S}_0$ (E1)			
Breit Pert.; VP. Pert.	1.071×10^6	3.520×10^6	1.947×10^6
Breit Pert.; VP SC	1.073×10^6	3.526×10^6	1.954×10^6
Breit SC; VP Pert.	1.062×10^6	3.501×10^6	1.920×10^6
Breit SC; VP SC	1.064×10^6	3.507×10^6	1.927×10^6
$7s7p\ ^1\mathrm{P}_1 \rightarrow 7s^2\ ^1\mathrm{S}_0$ (E1)			
Breit Pert.; VP. Pert.	2.705×10^8	3.500×10^8	3.680×10^8
Breit Pert.; VP SC	2.697×10^8	3.559×10^8	3.738×10^8
Breit SC; VP Pert.	2.711×10^8	3.509×10^8	3.686×10^8
Breit SC; VP SC	2.704×10^8	3.568×10^8	3.743×10^8
$7s7p\ ^3\mathrm{P}_2 \rightarrow 7s^2\ ^1\mathrm{S}_0$ (M2)			
Breit Pert.; VP. Pert.	1.717×10^{-4}	5.187×10^{-4}	5.492×10^{-4}
Breit Pert.; VP SC	1.713×10^{-4}	5.173×10^{-4}	5.477×10^{-4}
Breit SC; VP Pert.	1.721×10^{-4}	5.200×10^{-4}	5.513×10^{-4}
Breit SC; VP SC	1.717×10^{-4}	5.187×10^{-4}	5.499×10^{-4}

Table 7. Transition energies and transition rates to the ground state $5f^{15}6d^{10}7s^27p^6\ ^1\mathrm{S}_0$ of eka-radon (element 118). The transition values from states labeled with ^{c} were calculated with correlation up to $6f$, as well as the ground state.

Initial state			Transition energy (eV)	Transition rate (s^{-1})
$5f^{15}\ 6d^{10}\ 7s^2\ 7p^5\ 7d$	$^3\mathrm{D}_1 +^3\mathrm{P}_1$	^{c}	10.43	9.86×10^8
	$^3\mathrm{P}_1$	^{c}	6.81	5.53×10^7
	$^3\mathrm{D}_1 +^1\mathrm{P}_1$	^{c}	7.2	9.98×10^6
	$^3\mathrm{P}_2$		6.08	1.41×10^{-2}
	$^3\mathrm{F}_2$		16.95	1.11×10^{-2}
	$^3\mathrm{F}_3$		6.15	1.30×10^{-3}
	$^1\mathrm{D}_2$		6.25	1.10×10^{-3}
	$^3\mathrm{D}_3$		6.22	7.52×10^{-4}
	$^3\mathrm{F}_4$		6.01	3.91×10^{-14}
	$^3\mathrm{P}_0$	^{c}	6.64	
$5f^{15}\ 6d^{10}\ 7s^27p^58s$	$^1\mathrm{P}_1$	^{c}	4.73	2.04×10^8
	$^3P_2$	^{c}	4.3	2.04×10^{-3}

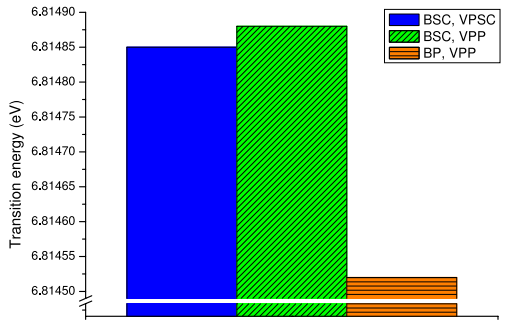

Fig. 10. (Color online) Changes in the $7p^58s\ ^3\mathrm{P}_1 \rightarrow 7s^27p^6\ ^1\mathrm{S}_0$ transition energy with respect to the approximation made, for element 118. BSC: Breit self-consistent. VPSC: Uelhing potential self consistent. BP: Breit in perturbation. VPP: Uelhing vacuum polarization in perturbation.

affected by the inclusion of these interactions in the SCF. This is illustrated in Figure 10 that shows the transition energy values for $7p^57d\ ^3\mathrm{P}_1$ transition.

5 Relativistic and QED effects on Landé factors, atomic radii and electronic densities

Although transition energies and probabilities, as well as ionization potential, are important quantities, it is interesting to study relativistic and QED effects on other atomic parameters, like Landé g-factors, atomic radii and electronic densities. Landé factors, which define the strength of the coupling of an atom to a magnetic field, can help characterize a level.

In some experiments concerning superheavy elements, singly ionized atoms are drifted in a gas cell, under the influence of an electric field. The drift speed can be related, in first approximation, to the charge distribution radius of the ion [75,76]. In this context, it can also be interesting to look at the atomic density, and see how it is affected by relativistic and QED effects. In that case, though, we can only get a feeling of this effect by comparing densities calculated with and without the Breit interaction self-consistent, or with and without the Uehling potential

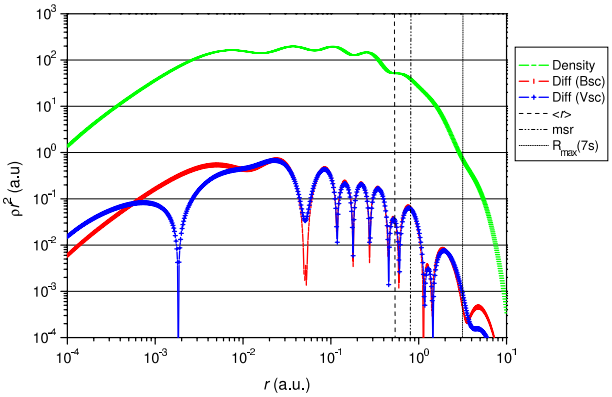

Fig. 11. (Color online) Total electronic density of Fm^+. The vertical lines represents, from left to right the mean radius, the mean spherical radius ("rms") and the mean radius of the outermost orbital ($7s$). "Density": total electronic density equation (10). "Diff (Bsc)": absolute value of the variation in the density due to the inclusion of the Breit interaction in the SCF. "Diff (Vsc)": absolute value of the variation in the density due to the inclusion of the Uehling potential in the differential equations (NB: the dip in the curve correspond to sign changes of the correction).

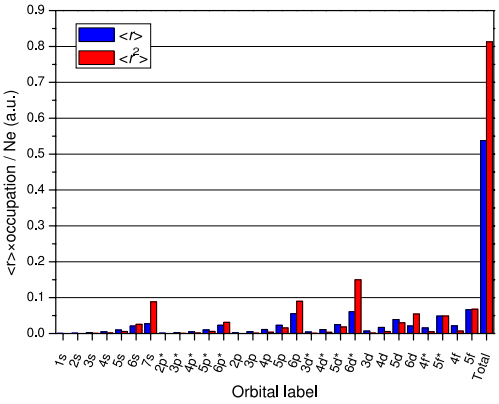

Fig. 12. (Color online) Contribution to the mean radius $\langle r^{(p)}_{\text{at.}}\rangle$ to Sg^+ of individual values of $\varpi_i\langle r^{(p)}_{n_i,l_i,j_i}\rangle$ for the different orbitals and $p = 1$ and 2, together with the total values on the right. Stared orbital labels correspond to the orbital with $j = l - \frac{1}{2}$.

included in the differential equation. There is currently no formalism that would enable to account for changes in the wavefunction related to the self-energy.

We define the radial electronic density as

$$r^2\rho(r) = \int d\Omega r^2 \rho(r,\Omega) = \sum_{i\in\text{occ.orb.}} \varpi_i \left(P_i(r)^2 + Q_i(r)^2\right), \quad (10)$$

where P and Q are defined in equation (7), and the ϖ_i are the orbital effective occupation numbers,

$$\varpi_i = \sum_j c_j^2 n_j^i, \quad (11)$$

where the sum extend over all configuration containing orbital i, and n_j^i is the occupation number of this orbital in the configuration j. The density is normalized to $\int_0^\infty drr^2\rho(r) = N_e$, where N_e is the number of electrons in the atom or ion.

The effect of the Breit interaction and vacuum polarization on the charge density of the ground state of Fm^+ ($[\text{Rn}]5f^{12}6s$) is shown in Figure 11. The inclusion of both contributions leads to local changes of around 1% in the charge density. It is rather unexpected that both contribution extend their effects way pass their range, in particular for the vacuum polarization potential, which has a very small contribution for $r > 1/\alpha = 0.0073$ a.u.

Charge distribution can be described in a number of ways, and the definition of atomic or ionic radius has evolved over the years. Slater noticed a long time ago the correlation between the value of the maximum charge density of the outermost core electron shell and the ionic radius of an atom [77]. Such a definition, however, does not provide a way to take into account mixing of outer shell in MCDF calculations. Other authors have chosen either the mean radius of a specific orbital $\langle r_{n,l,j}\rangle$ [78] or weighted mean radius [79]. Results have been obtained for bohrium and hassium. It is not at all obvious either than what is true in crystals must be valid for singly charged ions drifting in a gas. Here we have evaluated four different quantities and their dependence in the Breit interaction and vacuum polarization. We have evaluated the position of the maximum density of the outermost orbital, the mean radius of the outermost orbital $\langle r_{n,l,j}\rangle$, the atom mean radius, and the atom mean spherical radius. The two first quantities have been tested in detail, but they cannot represent the ionic radius when one has a complex outer shell structure or when one calculate correlation. The mean radius of the atom is represented as

$$\langle r^{(p)}_{\text{at.}}\rangle = \frac{1}{N_e}\int_0^\infty drr^p r^2\rho(r) = \frac{1}{N_e}\sum_{i\in\text{occ.orb.}} \varpi_i\langle r^{(p)}_{n_i,l_i,j_i}\rangle \quad (12)$$

for $p = 1$, and the mean spherical radius is obtained as $\sqrt{\langle r^{(2)}_{\text{at.}}\rangle}$. Both can be calculated in a MCDF model, as the ϖ_i contain both the occupation numbers and the mixing coefficients. As an example, we have plotted the contribution to $\langle r^{(p)}_{\text{at.}}\rangle$ to Sg^+ in Figure 12 of individual values of $\varpi_i\langle r^{(p)}_{n_i,l_i,j_i}\rangle$ for the different orbitals. Contrary to the individual orbitals quantities or to the average performed only on the outer shell, like in reference [9], both quantities have sizeable contributions from several outer shells. The $7s$, $6p$, $5f$ and $6d$ contribute significantly to both the mean and the mean spherical atomic radius, but the contribution of the $6d$ orbitals is more dominant for the mean spherical radius. The results for singly charged ions with

Table 8. Singly ionized atom radii (a.u.) for lanthanide $57 \leq Z \leq 71$ and actinide and transactinide $90 \leq Z \leq 108$.

Z	Config.	Label	$\langle r \rangle$	$\sqrt{\langle r^2 \rangle}$	outer orb. lab.	$R_{\max}$	$\langle 4f_{5/2} \rangle$	$\langle 4f_{7/2} \rangle$	$\langle 5d3/2 \rangle$	$\langle 5d_{7/2} \rangle$	$\langle 6s_{1/2} \rangle$
57	$5d^2$	$^3F_2$	0.6903	1.0365	$5d$	2.2820			2.8629	2.8900	
58	$4f5d^2$	$^4H_{7/2}$	0.6789	1.0121	$5d$	2.2005	1.0862	1.1033	2.7568	2.7949	
59	$4f^36s$	$^5I_4$	0.6750	1.0458	$6s$	3.8004	1.0589	1.0667			4.2924
60	$4f^46s$	$^6I_{7/2}$	0.6646	1.0256	$6s$	3.7359	1.0054	1.0190			4.2252
61	$4f^56s$	$^7H_2$	0.6544	1.0062	$6s$	3.6741	0.9624	0.9796			4.1608
62	$4f^66s$	$^8F_{1/2}$	0.6442	0.9874	$6s$	3.6171	0.9249	0.9392			4.1012
63	$4f^76s$	$^9S_4$	0.6342	0.9692	$6s$	3.5627	0.8920	0.8999			4.0438
64	$4f^75d6s$	$^{10}D_{5/2}$	0.6357	0.9708	$6s$	3.3408	0.8218	0.8221	2.4547	2.4846	3.7930
65	$4f^96s$	$^7H_8$	0.6162	0.9373	$6s$	3.4711	0.8502	0.8541			3.9568
66	$4f^{10}6s$	$^6I_{17/2}$	0.6074	0.9219	$6s$	3.4289	0.8254	0.8345			3.9163
67	$4f^{11}6s$	$^5I_8$	0.5987	0.9070	$6s$	3.3871	0.8022	0.8165			3.8758
68	$4f^{12}6s$	$^4H_{13/2}$	0.5903	0.8926	$6s$	3.3464	0.7804	0.7995			3.8359
69	$4f^{13}6s$	$^3F_4$	0.5820	0.8786	$6s$	3.3070	0.7605	0.7811			3.7976
70	$4f^{14}6s$	$^2S_{1/2}$	0.5739	0.8649	$6s$	3.2699	0.7430	0.7613			3.7611
71	$4f^{14}6s^2$	$^1S_0$	0.5876	0.9133	$6s$	2.9761	0.6922	0.7057			3.4229
							$\langle 5f_{5/2} \rangle$	$\langle 5f_{7/2} \rangle$	$\langle 6d_{3/2} \rangle$	$\langle 6d_{7/2} \rangle$	$\langle 7s_{1/2} \rangle$
90	$5f^26d$	$^4K_{11/2}$	0.5873	0.9117	$6d$	2.5751	1.96004	1.95812	3.16141	3.18613	
91	$5f^26d7s$	$^5K_5$	0.5977	0.9521	$7s$	3.5491	1.54181	1.57544	2.85704	2.9741	3.99617
92	$5f^36d7s$	$^6L_{11/2}$	0.5926	0.9377	$7s$	3.4779	1.42706	1.44552	2.78857	2.86351	3.92351
93	$5f^46d7s$	$^7L_5$	0.5873	0.9239	$7s$	3.4116	1.3478	1.36699	2.72666	2.79424	3.85537
94	$5f^56d7s$	$^8K_{7/2}$	0.5821	0.9107	$7s$	3.3498	1.28511	1.30541	2.67874	2.73928	3.7917
95	$5f^77s$	$^9S_4$	0.5699	0.8822	$7s$	3.4279	1.27013	1.29869			3.8992
96	$5f^77s^2$	$^8S_{7/2}$	0.5805	0.9217	$7s$	3.2104	1.16578	1.18716			3.65864
97	$5f^86d7s$	$^9G_7$	0.5670	0.8761	$7s$	3.1840	1.14449	1.16614	2.62581	2.688	3.62195
98	$5f^{10}7s$	$^6I_{17/2}$	0.5553	0.8493	$7s$	3.2905	1.14462	1.18171			3.77066
99	$5f^{11}7s$	$^5I_8$	0.5503	0.8385	$7s$	3.2461	1.10705	1.14777			3.72772
100	$5f^{12}7s$	$^2H_{11/2}$	0.5456	0.8293	$7s$	3.2294	1.07281	1.11537			3.72114
101	$5f^{13}7s$	$^3F_4$	0.5403	0.8174	$7s$	3.1625	1.0417	1.08491			3.64662
102	$5f^{14}7s$	$^2S_{1/2}$	0.5353	0.8071	$7s$	3.1235	1.01352	1.05406			3.6087
103	$5f^{14}7s^2$	$^1S_0$	0.5435	0.8385	$7s$	2.8837	0.95846	0.990419			3.32578
104	$5f^{14}6d7s^2$	$^2D_{3/2}$	0.5441	0.8392	$7s$	2.7464	0.917421	0.941578	2.33571		3.16377
105	$5f^{14}6d^27s^2$	$^3F_2$	0.5436	0.8355	$7s$	2.6309	0.881333	0.900734	2.17264	2.25313	3.02942
106	$5f^{14}6d^47s$	$^6D_{1/2}$	0.5376	0.8127	$7s$	2.5150	0.850008	0.867203	2.11798	2.21807	2.87277
107	$5f^{14}6d^47s^2$	$^5D_0$	0.5409	0.8240	$7s$	2.4351	0.820103	0.834045	1.95902	2.01018	2.80344
108	$5f^{14}6d^57s^2$	$^6S_{5/2}$	0.5396	0.8183	$7s$	2.3426	0.790744	0.807474	1.86004	1.95516	2.69468

Table 9. Correlation effects on the mean radius and mean spherical radius of No.

	$\langle r \rangle$ (a.u.)	var.	$\sqrt{\langle r^2 \rangle}$ (a.u.)	var.
Ra$5f^{14}7s^2\ ^1S_0$	0.574391		0.932605	
+ excit. of $7s \rightarrow 7p$, $6d$	0.573724	−0.12%	0.928191	−0.47%
+ excit. of $7s$, $5f \rightarrow 7p$, $6d$	0.573309	−0.19%	0.925313	−0.78%

$57 \leq Z \leq 71$ and $90 \leq Z \leq 108$ are presented in Table 8 and plotted in Figure 13. The comparison between mean radius and mean spherical radius with the Breit interaction in the SCF process with Coulomb values, shows changes around 0.04% to 0.08% depending on the atomic number. Self-consistent vacuum polarization has an effect 2 to 4 times smaller, depending on the element. We emphasize the fact that we used for the ion the configuration corresponding to the ground state of a Dirac-Fock calculation (i.e., without correlation), as given in [6]. For a few elements, the physical ground state configuration, as given for example on the NIST database, is different.

We have used the definition above to evaluate the effect of correlation on the ion radii. The calculation has been performed on neutral nobelium ($Z = 102$). The results are presented in Table 9. One can see that the radius of maximum density follows exactly the trend of the mean radius of the outer orbital. However the atomic mean radius and mean spherical radius follow a different trend.

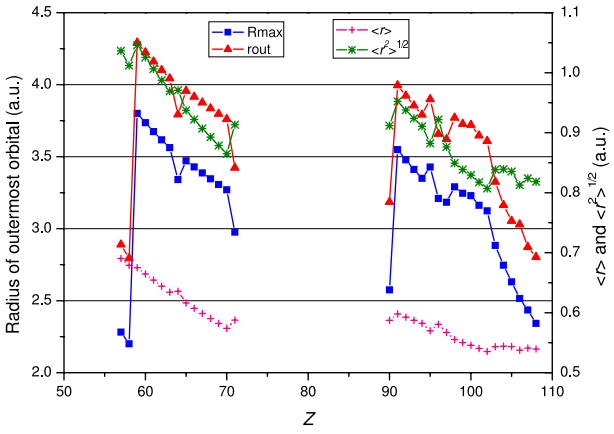

Fig. 13. (Color online) Variation of $\langle r \rangle$, $\sqrt{\langle r^2 \rangle}$ (right scale), of the radius of the outermost orbital $\langle r_{\rm out} \rangle$ and of the maximum of the charge density of the outer orbital ($R_{\max}$ dens.) (left scale) as a function of the atomic number Z.

Table 10. Comparison between different definition of the ionic radii and experiment. We define the average radius of $5f$ orbitals as $\langle r_{5f}\rangle = (6\langle r_{5f_{5/2}}\rangle + 8\langle r_{5f_{7/2}}\rangle)/14$.

	Exp.			Theo.
$\Delta r_{\mathrm{Am}^+-\mathrm{Pu}^+}$[75]	-3.1%	($\pm$ 1.3%)	$\langle r_{\mathrm{At.}}\rangle$	-2.1%
			$\sqrt{\langle r^2_{\mathrm{At.}}\rangle}$	-3.1%
			$\langle r_{5f}\rangle$	-0.8%
			$\langle r_{7s}\rangle$	2.8%
$\Delta r_{\mathrm{Fm}^+-\mathrm{Cf}^+}$ [18]	-2.0%		$\langle r_{\mathrm{At.}}\rangle$	-1.7%
			$\sqrt{\langle r^2_{\mathrm{At.}}\rangle}$	-2.4%
			$\langle r_{5f}\rangle$	-5.9%
			$\langle r_{7s}\rangle$	-1.3%

There has been two experiments measuring drift time of singly ionized transuranic elements in gases. One measured the relative velocity of Am^+ with respect to Pu^+ [75] and an other one measured the same quantity for Cf^+ and Fm^+ [18]. The results of these experiments are expressed as

$$\Delta r_{A-B} = \frac{r_A - r_B}{r_B}. \tag{13}$$

The experiments above provide $\Delta r_{\mathrm{Am}^+-\mathrm{Pu}^+} = -3.1 \pm 1.3\%$ and $\Delta r_{\mathrm{Fm}^+-\mathrm{Cf}^+} = -2\%$ respectively, which shows a shrinkage of Am as compares to Pu and of Fm as compared to Cf. The comparison between these experiments and the calculation of singly charged ion radii from Table 8 is shown in Table 10. Although it is difficult to draw any firm conclusion from so few data, it seems that $\sqrt{\langle r^{(2)}_{\mathrm{at.}}\rangle}$ reproduces best the experiment, followed by $\langle r^{(1)}_{\mathrm{at.}}\rangle$. We want to point out that the $\langle r_{7s}\rangle$ values for neutral atom, from reference [5], or ours, which are in good agreement gives a -1.5% change for Am/Pu and -3.0% for Fm/Cf, compare well with experiment. The $7s$ radius of the singly charged ions, as shown in Table 8, increases when going from Am to Pu, thus leading to a ratio of the wrong sign, while the $5f$ average radius, or the global atomic radii as defined here all show the right trend. The change of behavior for Am, is due to the relative diminution of the $l(l+1)/r^2$ barrier compared to the Coulomb potential as a function of Z. The $5f$ radius reduces then strongly, leading to the change of the structure of the ground configuration, and to the change of the radius of the $7s$ orbital.

QED corrections on Landé factors of one and three electron atoms have been studied in great details in the last few years, because of the increase in experimental accuracy associated with the use of Penning traps in a new series of experiments [80,81]. These experiments provided a strong incentives to evaluate very accurately QED corrections on Landé factors, beyond the one due to the anomalous magnetic moment of the electron [82–89]. To our knowledge, there has been only one calculation dealing with QED corrections in heavy elements, in which the Feynman diagrams corresponding to self-energy and other corrections were evaluated. This calculation concerned alkali elements up to francium ($Z = 87$) [90]. Here we deal with much more complex system, with several open shells, and we calculate QED corrections due to the inclusion of the Breit interaction and of the vacuum polarization in the SCF, as well as the contribution from the electron anomalous moment. The coupling of an atom with a magnetic moment μ to a homogeneous magnetic field $\boldsymbol{B}$ gives an energy change

$$\Delta E = -\mu \cdot \boldsymbol{B} \tag{14}$$

where $\mu = -g_J \mu_B \boldsymbol{J}$, g_J being the Landé factor and μ_B the Bohr magneton. The anomalous electron magnetic moment corrections can be written (see, e.g., [91] and reference therein) as

$$\Delta g_J = (g-2)\frac{\langle J||\beta\boldsymbol{\Sigma}||J\rangle}{\sqrt{J(J+1)(2J+1)}} \tag{15}$$

where $g = 2\left(1 + \frac{\alpha}{\pi} + \cdots\right)$ is the electron magnetic moment, β and Σ are 4×4 matrices, $\beta = \begin{pmatrix} I & 0 \\ 0 & I \end{pmatrix}$ and $\boldsymbol{\Sigma} = \begin{pmatrix} \boldsymbol{\sigma} & 0 \\ 0 & \boldsymbol{\sigma} \end{pmatrix}$ where I is a 2×2 identity matrix and $\boldsymbol{\sigma}$ are Pauli matrices.

As an example, we illustrate the different effects by evaluating the Landé g-factors for the ground configuration of neutral actinide and transactinide up to $Z = 106$, and of singly ionized lanthanide, actinide and transactinide up to $Z = 106$. The results are displayed in Table 11 for neutral atoms and in Table 12, for singly ionized atoms. The ground configuration of neutral atom comes from [92]. For singly ionized atoms, it has been taken from reference [6] for Z up to 106 and from [9] for $Z = 107$ and 108. Depending on the outer shell structures, the QED corrections can be dominated by either the $g-2$ correction or the Breit correction (order of 0.1% of the Landé factor). The vacuum polarization correction is at best one order of magnitude smaller at $Z = 106$.

In Table 13, we present correlation effects on the Landé g-factor of the lowest levels of No, evaluated with the same wavefunctions as in Section 4.3, with the Breit operator in the SCF process. The effect of correlation ranges from 0.6% to 0.02% depending on the level.

6 Conclusions

In this work we have evaluated the effects of self-consistent Breit interaction and vacuum polarization on level energies, transition energies and probabilities, and Landé g-factors on super-heavy elements. We have also studied their effect on orbitals and atomic charge distribution radii and found very large effects on highly charged ions. We have found some hints, when studying Be-like ions, of rather strong non-perturbative correlation effects for $Z \approx 128$. For neutral or quasi-neutral systems, self-consistent Breit interaction and vacuum polarization have a small but noticeable effects on Landé factor and transition rates, which could be felt experimentally. Transition energies, on the other hand, are heavily dominated by

Table 11. QED [Eq. (15)], Breit and Uehling corrections on Landé g-factors of neutral atoms with $90 \leq Z \leq 106$.

Z	Conf.	Label	Landé (Coul.)	QED corr.	Breit contr.	Uehl. corr.	Total
90	$6d^2 7s^2$	$^3\mathrm{F}_2$	0.68158912	−0.00073903	−0.00031059	−0.00002136	0.68051814
91	$5f^2 6d 7s^2$	$^4\mathrm{K}_{11/2}$	0.81847964	−0.00042068	−0.00020095	−0.00001531	0.81784271
92	$5f^3 6d 7s^2$	$^5\mathrm{L}_6$	0.73962784	−0.00060501	−0.00090733	−0.00001069	0.73810480
93	$5f^4 6d 7s^2$	$^6\mathrm{L}_{11/2}$	0.63735126	−0.00084251	−0.00108525	−0.00000780	0.63541570
94	$5f^6 7s^2$	$^7\mathrm{F}_0$					
95	$5f^7 7s^2$	$^8\mathrm{S}_{7/2}$	1.96702591	0.00224893	0.00193804	0.00000967	1.97122254
96	$5f^7 6d 7s^2$	$^9\mathrm{D}_2$	2.60336698	0.00372915	0.00336317	0.00002669	2.61048600
97	$5f^9 7s^2$	$^6\mathrm{H}_{15/2}$	1.29988703	0.00070147	0.00177562	0.00000642	1.30237054
98	$5f^{10} 7s^2$	$^5\mathrm{I}_8$	1.22357731	0.00052300	0.00108516	0.00000375	1.22518921
99	$5f^{11} 7s^2$	$^4\mathrm{I}_{15/2}$	1.18834647	0.00043997	0.00047015	0.00000159	1.18925817
100	$5f^{12} 7s^2$	$^3\mathrm{H}_6$	1.16189476	0.00037811	0.00019838	0.00000062	1.16247187
101	$5f^{13} 7s^2$	$^2\mathrm{F}_{7/2}$	1.14180915	0.00033132	0.00005605	0.00000020	1.14219672
102	$5f^{14} 7s^2$	$^1\mathrm{S}_0$					
103	$5f^{14} 7s^2 7p$	$^2\mathrm{P}_{1/2}$	0.66661695	−0.00077309	0.00003007	0.00000003	0.66587396
104	$5f^{14} 6d^2 7s^2$	$^3\mathrm{P}_0$					
104	$5f^{14} 7s^2 7p^2$	$^3\mathrm{F}_2$	0.69055158	−0.00071837	−0.00035975	−0.00006392	0.68940954
105	$5f^{14} 6d^3 7s^2$	$^4\mathrm{F}_{3/2}$	0.45467514	−0.00126763	−0.00122595	−0.00016406	0.45201750
106	$5f^{14} 6d^4 7s^2$	$^5\mathrm{D}_0$					

Table 12. QED [Eq. (15)], Breit and Uehling corrections on Landé g-factors of the ground configuration of singly ionized atoms with $57 \leq Z \leq 71$ and $90 \leq Z \leq 108$.

Z	Conf.	Label	Landé (Coul.)	QED corr.	Breit contr.	Uehl. corr.	Total
57	$5d^2$	$^3\mathrm{F}_2$	0.66973929	−0.00076609	−0.00012975	−0.00000075	0.66884270
58	$4f 5d^2$	$^4\mathrm{H}_{7/2}$	0.71736392	−0.00065375	0.00039406	−0.00000787	0.71709635
59	$4f^3 6s$	$^5\mathrm{I}_4$	0.60262203	−0.00092068	−0.00031540	−0.00000026	0.60138569
60	$4f^4 6s$	$^6\mathrm{I}_{7/2}$	0.44690832	−0.00128150	−0.00029522	−0.00000023	0.44533137
61	$4f^5 6s$	$^7\mathrm{H}_2$	0.00677005	−0.00230319	−0.00086739	−0.00000061	0.00359886
62	$4f^6 6s$	$^8\mathrm{F}_{1/2}$	3.95749786	0.00687585	0.00701619	0.00001509	3.97140499
63	$4f^7 6s$	$^9\mathrm{S}_4$	1.99480186	0.00230987	0.00035927	0.00000034	1.99747133
64	$4f^7 5d 6s$	$^{10}\mathrm{D}_{5/2}$	2.56089325	0.00362452	0.00067458	0.00000119	2.56519354
65	$4f^9 6s$	$^7\mathrm{H}_8$	1.36838651	0.00085813	0.00067487	0.00000040	1.36991992
66	$4f^{10} 6s$	$^6\mathrm{I}_{17/2}$	1.28727646	0.00067021	0.00068999	0.00000039	1.28863705
67	$4f^{11} 6s$	$^5\mathrm{I}_8$	1.24630282	0.00057447	0.00033068	0.00000018	1.24720815
68	$4f^{12} 6s$	$^4\mathrm{H}_{13/2}$	1.22865909	0.00053325	0.00015805	0.00000008	1.22935048
69	$4f^{13} 6s$	$^3\mathrm{F}_4$	1.24882255	0.00057982	0.00006252	0.00000004	1.24946493
70	$4f^{14} 6s$	$^2\mathrm{S}_{1/2}$	1.99992029	0.00231927	−0.00000949	−0.00000006	2.00223002
71	$4f^{14} 6d^2$	$^1\mathrm{S}_0$					
90	$5f^2 6d$	$^4\mathrm{K}_{11/2}$	0.80868853	−0.00044409	−0.00040145	−0.00001738	0.80782561
91	$5f^2 6d 7s$	$^5\mathrm{K}_5$	0.69942415	−0.00069727	−0.00041498	−0.00003386	0.69827803
92	$5f^3 6d 7s$	$^6\mathrm{L}_{11/2}$	0.63834785	−0.00083965	−0.00081792	−0.00001647	0.63667382
93	$5f^4 6d 7s$	$^7\mathrm{L}_5$	0.52126261	−0.00111157	−0.00103625	−0.00001135	0.51910344
94	$5f^5 6d 7s$	$^8\mathrm{K}_{7/2}$	0.26613829	−0.00170714	−0.00271582	−0.00002210	0.26169324
95	$5f^7 7s$	$^9\mathrm{S}_4$	1.97238902	0.00226041	0.00159104	0.00001036	1.97625083
96	$5f^7 7s^2$	$^8\mathrm{S}_{7/2}$	1.95878066	0.00223118	0.00242861	0.00001187	1.96345232
97	$5f^8 6d 7s$	$^9\mathrm{G}_7$	1.48746928	0.00113601	0.00161739	0.00001838	1.49024105
98	$5f^{10} 7s$	$^6\mathrm{I}_{17/2}$	1.27036131	0.00063117	0.00097651	0.00000581	1.27197480
99	$5f^{11} 7s$	$^5\mathrm{I}_8$	1.23940637	0.00055819	0.00042388	0.00000222	1.24039065
100	$5f^{12} 7s$	$^2\mathrm{H}_{11/2}$	1.09903182	0.00023261	0.00025286	0.00000531	1.09952260
101	$5f^{13} 7s$	$^3\mathrm{F}_4$	1.24906758	0.00057982	0.00004304	0.00000013	1.24969057
102	$5f^{14} 7s$	$^2\mathrm{S}_{1/2}$	1.99988521	0.00231927	−0.00002001	−0.00000035	2.00218413
103	$5f^{14} 7s^2$	$^1\mathrm{S}_0$					
104	$5f^{14} 6d 7s^2$	$^2\mathrm{D}_{3/2}$	0.79977826	−0.00046385	0.00005358	0.00000012	0.79936810
105	$5f^{14} 6d^2 7s^2$	$^3\mathrm{F}_2$	0.70320927	−0.00068901	−0.00043211	−0.00005473	0.70203342
106	$5f^{14} 6d^4 7s$	$^6\mathrm{D}_{1/2}$	3.19780436	0.00510655	0.00311970	0.00051784	3.20654845
107	$5f^{14} 6d^4 7s^2$	$^5\mathrm{D}_0$					
108	$5f^{14} 6d^5 7s^2$	$^6\mathrm{S}_{5/2}$	1.87088576	0.00203080	0.00399742	0.00034326	1.87725723

Table 13. Correlation effect on the Landé g-factor of the first excited states of nobelium.

Level	$7s7p^3\mathrm{P}_1$	$7s7p^1\mathrm{P}_1$	$7s7p^3\mathrm{P}_2$
DF	1.49073	1.00932	1.50111
7, $7p$ exc. $\rightarrow$ $7p$, $6d$	1.47691	1.02829	1.50027
7, $7p$, $5f$ exc. $\rightarrow$ $7p$, $6d$	1.48845	1.01507	1.50080

Coulomb correlation. This is rather good news, since treating the Breit interaction self-consistently obliges to evaluate magnetic and retardation integrals during the SCF process, which are about one order of magnitude more numerous than Coulomb ones, leading to calculations that cannot fit on even on the largest computers available today, even with relatively small configuration space.

We have shown that very large non-relativistic offset may affect the fine structure separation of elements with several open shells. This should be carefully taken into account to avoid providing completely wrong results with all-order methods. We have also shown that the inclusion of the Breit interaction in the SCF process, because it get mixing coefficients closer to the jj limit, can noticeably complicate numerical convergence.

Laboratoire Kastler Brossel is Unité Mixte de Recherche du CNRS n° C8552. This research was partially supported by the FCT projects POCTI/FAT/44279/2002 and POCTI-/0303/2003 (Portugal), financed by the European Community Fund FEDER, and by the French-Portuguese collaboration (PESSOA Program, Contract n° 10721NF). One of us (P.I.) thanks M. Sewtz for several discussions on this subject. The 8-processors workstation used for the calculations has been provided by an "infrastructure" grant from the "Ministère de La Recherche et de l'Enseignement Supérieur".

References

1. Y.T. Oganessian et al., Phys. Rev. C **74**, 044602 (2006)
2. S. Hofmann, G. Münzenberg, Rev. Mod. Phys. **72**, 733 (2000)
3. J.B. Mann, J.T. Waber, J. Chem. Phys. **53**, 2397 (1970)
4. B. Fricke, J.T. Waber, Actinides Rev. **1**, 433 (1971)
5. J.P. Desclaux, At. Data Nucl. Data Tables **12**, 311 (1973)
6. G.C. Rodrigues, P. Indelicato, J.P. Santos, P. Patté, F. Parente, At. Data Nucl. Data Tables **86**, 117 (2004)
7. J.P. Santos, G.C. Rodrigues, J.P. Marques, F. Parente, J.P. Desclaux, P. Indelicato, Eur. Phys. J. D **37**, 201 (2006)
8. N. Gaston, P. Schwerdtfeger, W. Nazarewicz, Phys. Rev. A **66**, 062505 (2002)
9. E. Johnson, B. Fricke, T. Jacob, C.Z. Dong, S. Fritzsche, V. Pershina, J. Chem. Phys. **116**, 1862 (2002)
10. E. Eliav, U. Kaldor, Y. Ishikawa, Phys. Rev. Lett. **74**, 1079 (1995)
11. E. Eliav, U. Kaldor, Y. Ishikawa, Phys. Rev. A **52**, 291 (1995)
12. E. Eliav, U. Kaldor, Y. Ishikawa, Phys. Rev. Lett. **77**, 5350 (1996)
13. M. Seth, P. Schwerdtfeger, M. Dolg, K. Faegri, B.A. Hess, U. Kaldor, Chem. Phys. Lett. **250**, 461 (1996)
14. E. Eliav, U. Kaldor, Y. Ishikawa, Molec. Phys. **94**, 181 (1998)
15. A. Landau, E. Eliav, Y. Ishikawa, U. Kaldor, J. Chem. Phys. **114**, 2977 (2001)
16. A. Landau, E. Eliav, Y. Ishikawa, U. Kaldor, J. Chem. Phys. **115**, 2389 (2001)
17. E. Eliav, A. Landau, Y. Ishikawa, U. Kaldor, J. Phys. B: At. Mol. Opt. Phys. **35**, 1693 (2002)
18. M. Sewtz et al., Phys. Rev. Lett. **90**, 163002 (2003)
19. M. Sewtz, H. Backe, C.Z. Dong, A. Dretzke, K. Eberhardt, S. Fritzsche, C. Gruning, R.G. Haire, G. Kube, P. Kunz, Spectrochim. Acta B: At. Spectrosc. **58**, 1077 (2003)
20. H. Backe, A. Dretzke, S. Fritzsche, R. Haire, P. Kunz, W. Lauth, M. Sewtz, N. Trautmann, Hyperf. Int. **162**, 3 (2005)
21. S. Fritzsche, Eur. Phys. J. D **33**, 15 (2005)
22. Y. Zou, C.F. Fischer, Phys. Rev. Lett. **88**, 183001 (2002)
23. P. Indelicato, J. Desclaux, *Mcdfgme, a multiconfiguration dirac fock and general matrix elements program (release 2005)*, `http://dirac.spectro.jussieu.fr/mcdf` (2005)
24. J.P. Desclaux, Comp. Phys. Commun. **9**, 31 (1975)
25. J.P. Desclaux, in *Methods and Techniques in Computational Chemistry*, edited by E. Clementi (STEF, Cagliary, 1993), Vol. A: Small Systems of *METTEC*, p. 253
26. P. Indelicato, Phys. Rev. A **51**, 1132 (1995)
27. P. Indelicato, Phys. Rev. Lett. **77**, 3323 (1996)
28. O. Gorceix, P. Indelicato, Phys. Rev. A **37**, 1087 (1988)
29. E. Lindroth, A.M. Mårtensson-Pendrill, Phys. Rev. A **39**, 3794 (1989)
30. I. Angeli, At. Data Nucl. Data Tables **87**, 185 (2004)
31. P.O. Löwdin, Phys. Rev. **97**, 1474 (1955)
32. J.C. Slater, *Quantum Theory of Molecules and Solids*, Vol. 1 of *International Series in Pure and Applied Physics* (McGraw-Hill, New York, 1963)
33. P.J. Mohr, Ann. Phys. (N.Y.) **88**, 26 (1974)
34. P.J. Mohr, Ann. Phys. (N.Y.) **88**, 52 (1974)
35. P.J. Mohr, Phys. Rev. Lett. **34**, 1050 (1975)
36. P.J. Mohr, Phys. Rev. A **26**, 2338 (1982)
37. P.J. Mohr, Y.K. Kim, Phys. Rev. A **45**, 2727 (1992)
38. P. Indelicato, P.J. Mohr, Phys. Rev. A **46**, 172 (1992)
39. P. Indelicato, P.J. Mohr, Phys. Rev. A **58**, 165 (1998)
40. E.O. Le Bigot, P. Indelicato, P.J. Mohr, Phys. Rev. A **64**, 052508 (14) (2001)
41. K.T. Cheng, W.R. Johnson, Phys. Rev. A **14**, 1943 (1976)
42. G. Soff, P. Schlüter, B. Müller, W. Greiner, Phys. Rev. Lett. **48**, 1465 (1982)
43. P.J. Mohr, G. Soff, Phys. Rev. Lett. **70**, 158 (1993)
44. P. Indelicato, O. Gorceix, J.P. Desclaux, J. Phys. B: At. Mol Phys. **20**, 651 (1987)
45. P. Indelicato, J.P. Desclaux, Phys. Rev. A **42**, 5139 (1990)
46. S.A. Blundell, Phys. Rev. A **46**, 3762 (1992)
47. S.A. Blundell, Phys. Scr. **T46**, 144 (1993)
48. S.A. Blundell, Phys. Rev. A **47**, 1790 (1993)
49. P. Indelicato, P.J. Mohr, Phys. Rev. A **63**, 052507 (2001)
50. P. P., M. Tokman, L.N. Labzowsky, Phys. Rev. A **57**, R689 (1998)
51. L. Labzowsky, I. Goidenko, M. Tokman, P. Pyykkö, Phys. Rev. A **59**, 2707 (1999)
52. F.A. Parpia, C. Froese Fischer, I.P. Grant, Comp. Phys. Commun. **94**, 249 (1996)

53. E.A. Uehling, Phys. Rev. **48**, 55 (1935)
54. S. Boucard, P. Indelicato, Eur. Phys. J. D **8**, 59 (2000)
55. S. Klarsfeld, Phys. Lett. **66B**, 86 (1977)
56. P. Indelicato, A.M. Måtensson-Pendrill, W. Quint, J.P. Desclaux, Hyperf. Int. **146–147**, 127 (2003)
57. V.A. Yerokhin, P. Indelicato, V.M. Shabaev, Phys. Rev. Lett. **91**, 073001 (2003)
58. V.A. Yerokhin, P. Indelicato, V.M. Shabaev, Eur. Phys. J D **25**, 203 (2003)
59. V.A. Yerokhin, P. Indelicato, V.M. Shabaev, Phys. Rev. A **71**, 040101(R) (2005)
60. V.A. Yerokhin, P. Indelicato, V.M. Shabaev, JETP **101**, 280 (2005)
61. V.A. Yerokhin, P. Indelicato, V.M. Shabaev, Phys. Rev. Lett. **97**, 253004 (2006)
62. W.R. Johnson, C.D. Lin, Phys. Rev. A **14**, 565 (1976)
63. W.R. Johnson, J. Sapirstein, Phys. Rev. Lett. **57**, 1126 (1986)
64. P. Indelicato, F. Parente, R. Marrus, Phys. Rev. A **40**, 3505 (1989)
65. J.P. Desclaux, K.T. Cheng, Y.K. Kim, J. Phys. B: At. Mol. Phys. **12**, 3819 (1979), http://stacks.iop.org/0022-3700/12/3819
66. K.L. Vander Sluis, L.J. Nugent, Phys. Rev. A **6**, 86 (1972)
67. L.J. Nugent, K.L.V. Sluis, B. Fricke, J.B. Mann, Phys. Rev. A **9**, 2270 (1974)
68. J.P. Desclaux, B. Fricke, J. Phys. France **41**, 943 (1980)
69. K.N. Huang, Y.K. Kim, K.T. Cheng, J.P. Desclaux, Phys. Rev. Lett. **48**, 1245 (1982)
70. P. Indelicato, E. Lindroth, J.P. Desclaux, Phys. Rev. Lett. **94**, 013002 (2005)
71. E.O. Le Bigot, P. Indelicato, V. Shabaev, Phys. Rev. A **63**, 040501(R) (2001)
72. I. Lindgren, B. Åsén, S. Salomonson, A.M. Mårtensson-Pendrill, Phys. Rev. A **64**, 062505 (5) (2001)
73. A.N. Artemyev, V.M. Shabaev, V.A. Yerokhin, G. Plunien, G. Soff, Phys. Rev. A **71**, 062104 (2005)
74. P.J. Mohr, B.N. Taylor, Rev. Mod. Phys. **72**, 351 (2000)
75. H. Backe, A. Dretzke, R. Horn, T. Kolb, W. Lauth, R. Repnow, M. Sewtz, N. Trautmann, Hyperf. Int. **162**, 77 (2005)
76. M. Sewtz, M. Laatiaoui, D. Habs, Eur. Phys. J. D (2007)
77. J.C. Slater, J. Chem. Phys. **41**, 3199 (1964)
78. S. Siekierski, Comm. on Inorg. Chem. **19**, 121 (1997)
79. A. Bilewicz, Radiochim. Acta **88**, 833 (2000)
80. H. Häffner, T. Beier, N. Hermanspahn, H.J. Kluge, W. Quint, S. Stahl, J. Verdu, G. Werth, Phys. Rev. Lett. **85**, 5308 (2000)
81. J. Verdu, S. Djekic, S. Stahl, T. Valenzuela, M. Vogel, G. Werth, T. Beier, H.J. Kluge, W. Quint, Phys. Rev. Lett. **92**, 093002 (2004)
82. H. Persson, S. Salomonson, P. Sunnergren, I. Lindgren, Phys. Rev. A **56**, R2499 (1997)
83. T. Beier, I. Lindgren, H. Persson, S. Salomonson, P. Sunnergren, H. Häffner, N. Hermanspahn, Phys. Rev. A **62**, 032510 (2000)
84. V.A. Yerokhin, P. Indelicato, V.M. Shabaev, Phys. Rev. Lett. **89**, 143001 (2002)
85. T. Beier, P. Indelicato, V.M. Shabaev, V.A. Yerokhin, J. Phys. B: At. Mol. Opt. Phys. **36**, 1019 (2003)
86. D.A. Glazov, V.M. Shabaev, I.I. Tupitsyn, A.V. Volotka, V.A. Yerokhin, G. Plunien, G. Soff, Phys. Rev. A **70**, 062104 (2004)
87. K. Pachucki, U.D. Jentschura, V.A. Yerokhin, Phys. Rev. Lett. **93**, 150401 (2004)
88. V.A. Yerokhin, P. Indelicato, V.M. Shabaev, Phys. Rev. A **69**, 052503 (2004)
89. K. Pachucki, A. Czarnecki, U.D. Jentschura, V.A. Yerokhin, Phys. Rev. A **72**, 022108 (2005)
90. L. Labzowsky, I. Goidenko, P. Pyykkö, Phys. Lett. A **258**, 31 (1999)
91. K.T. Cheng, W.J. Childs, Phys. Rev. A **31**, 2775 (1985)
92. R. Dragoset, A. Musgrove, C. Clark, W. Martin, *Periodic Table: Atomic properties of the elements* (2003), http://physics.nist.gov/PhysRefData/PerTable/index.html